Low-field magnetoresistance in nanosized $La_{0.7}Sr_{0.3}MnO_3/Pr_{0.5}Sr_{0.5}MnO_3$ composites

J.-M. Liu[a)]
Laboratory of Solid State Microstructures, Nanjing University, Nanjing 210093, China and
Laboratory of Laser Technologies, Huazhong University of Science and Technology, Wuhan 430074, China

G. L. Yuan, H. Sang, Z. C. Wu, X. Y. Chen, Z. G. Liu, and Y. W. Du
Laboratory of Solid State Microstructures, Nanjing University, Nanjing 210093, China

Q. Huang and C. K. Ong
Department of Physics, National University of Singapore, Singapore 119260

(Received 24 October 2000; accepted for publication 2 January 2001)

Nanosized $La_{0.7}Sr_{0.3}MnO_3/Pr_{0.5}Sr_{0.5}MnO_3$ ($LSMO_{1-x}PSMO_x$) ceramic composites are prepared using solid-sate sintering. Their microstructural, electro- and magnetotransport properties are characterized by means of various techniques. It is found that the antiferromagnetic/ferromagnetic coupling between PSMO/LSMO at low temperature and the weak ferromagnetic order of PSMO at high temperature results in enhanced low-field magnetoresistance (LFMR) of the composites. With increasing temperature up to 250 K the observed LFMR decays more slowly than that for pure LSMO and this behavior may be explained by the spin coupling near boundaries between LSMO and PSMO grains. © *2001 American Institute of Physics.* [DOI: 10.1063/1.1350602]

The low-field magnetoresistance (LFMR) in perovskite manganite oxides is of special interests due to the fact that this effect may find potential applications in next generation of digital recording and sensing devices.[1–3] However, the problem that LFMR is too low under low magnetic field ($H \sim 10^2$ Oe) has been challenging researchers in this field. Furthermore, LFMR shows a rapid decaying with temperature T, unfavorable for device applications at room temperature. Very different from colossal magnetoresistance, LFMR originates from spin-polarized electron tunneling[3] instead of double-exchange mechanism.[4] Introduction of nonferromagnetic and insulating second phase into the microstructure would benefit to LFMR.[3,5–7] Enhanced LFMR in a number of perovskite manganites in which grain boundaries, porous structure, oxygen-deficient zones, and other second phases exist as barriers for electron tunneling was reported, while the single crystals and epitaxial thin films do not show considerable LFMR.[6,7] On one hand, these defects or second phases damage seriously the electrical conductivity (over six orders of magnitude and more).[8,9] Such high resistivity makes the application of the materials incompatible. On the other hand, the LFMR in polycrystalline samples is yet low, despite the conductivity remains acceptable.

In this letter we report sintering of nanosized $La_{0.7}Sr_{0.3}MnO_3/Pr_{0.5}Sr_{0.5}MnO_3$ ($LSMO_{1-x}PSMO_x$) ceramic composites and their enhanced LFMR property. LSMO is a ferromagnetic metal (FMM) up to $T=T_C \sim 360$ K, where T_C is the Curie point, but PSMO is an insulator of antiferromagnetic state (AFM) at low T (Neel point $T_N \sim 135$ K) and weak ferromagnetic (ferrimagnetic) state at $T>T_N$ with the FM-paramagnetic transition at $T=T_C \sim 260$ K.[10] Although PSMO shows very low LFMR, its decaying with T is much slower than that for LSMO, mainly because of the field-sensitive FM state. The spin coupling between the FM and AFM phases is believed to affect LFMR of nanosized $LSMO_{1-x}PSMO_x$ composites.

The $LSMO_{1-x}PSMO_x$ ($x=0-1.0$) ceramic composites were prepared by conventional solid-state sintering. First, LSMO (or PSMO) powders were prepared from a citrate gel. The single-phase LSMO and PSMO powders were obtained by calcining the gel in air at 700 °C for 24 h. Then the $LSMO_{1-x}PSMO_x$ composite pellets were obtained by mixing LSMO and PSMO powders, which were subsequently ground, pressed and sintered at 1150 °C for various times. Here the sintering time was essential to avoid at most the interfacial reaction between LSMO and PSMO, consequently prohibiting formation of $La_{0.7(1-x)}Pr_{0.5x}Sr_{0.3+0.2x}MnO_3$ phase. The optimized sintering time as determined from LFMR evaluation was ~500 min. The fine-step x-ray diffraction (XRD) and high-resolution scanning electron microscopy [(SEM), JSM-6300, JEOL, Japan] with energy dispersive x-ray analysis [(EDX) Sigma, KEVEX] were utilized to check the crystallinity, constitution and microstructure of the samples. The four-pad technique was used to evaluate the electrical resistivity with and without external magnetic field H. The maximum H was 3.0 kOe. The Oxford vibrating sampling magnetometer (VSM) was utilized to probe the magnetic property. All samples had the same volume and shape and the magnetometer was calibrated carefully before the measurement.

Figure 1 presents the XRD θ–2θ spectra of a series of $LSMO_{1-x}PSMO_x$ samples, where x takes 0.0, 0.1, 0.3, 0.5, 0.7, and 1.0 from bottom to top. The well-defined (110), (111), (200), (211), and (220) reflections are identified. The two inserts give the amplified (111) and (211) profiles in order to display the evolution of the peaks with varying x. The two vertical arrows label the positions of pure LSMO and PSMO reflections, respectively, from which one can

a)Electronic mail: liujm@nju.edu.cn

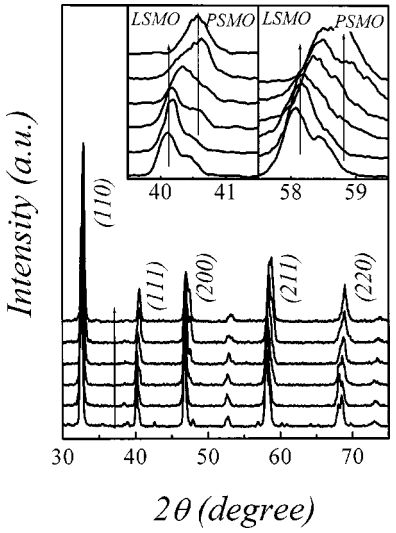

FIG. 1. XRD θ–2θ spectra of a series of $LSMO_{1-x}PSMO_x$ ceramic samples. The value of x takes 0.0, 0.1, 0.3, 0.5, 0.7, and 1.0 from bottom to top. The inserts give the local profiles of (111) and (211) reflections.

identify the two peaks for LSMO and PSMO, respectively, in particular as $x=0.3$ or 0.5. The sample seem to be the two-phase composite $LSMO_{1-x}PSMO_x$.

The second evidence to confirm the two-phase coexistence is given in Fig. 2, in which as an example the SEM image [Fig. 2(a)] plus the line-scanned spatial fluctuations of element La and Pr [Figs. 2(b) and 2(c)] for sample $x=0.5$ is presented. The as-probed spatial distribution of La and Pr shows significant fluctuations in submicron scale (~200 nm or less in wavelength). The one-to-one correspondence between the valleys of La (or Pr) and peaks of Pr (or La) can be establisehd too. Although the data may only be semiquantitative, the present result demonstrates that the sample indeed consists of nanosized LSMO and PSMO phases. Nevertheless, withstanding only the EDX data, the interfacial diffusion reaction between LSMO and PSMO grains cannot be excluded.

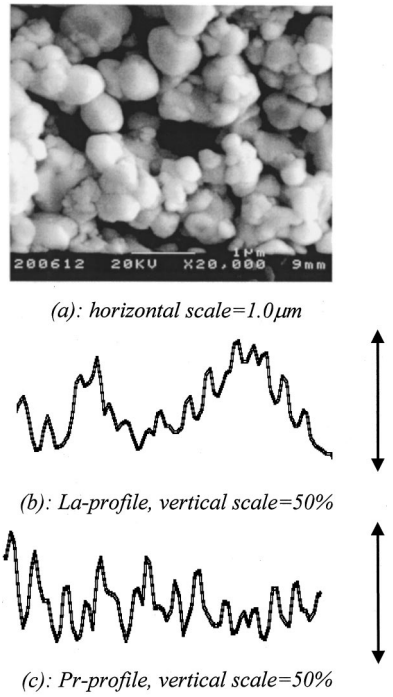

FIG. 2. (a) SEM image of $LSMO_{1-x}PSMO_x$ sample ($x=0.5$), and EDX line-scanned profiles of element La (b) and Pr (c) along horizontal axis.

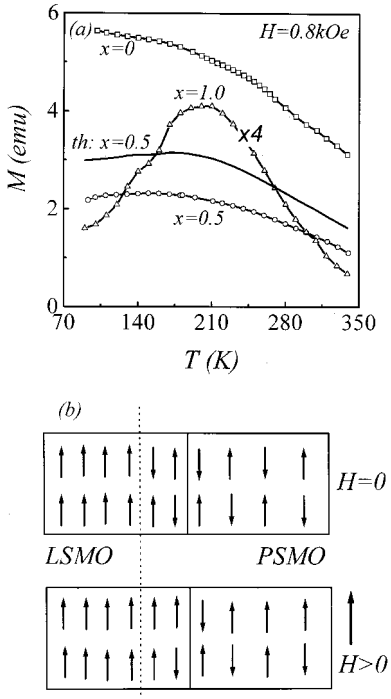

FIG. 3. (a) Magnetization M of $LSMO_{1-x}PSMO_x$ as $x=0.0$, 0.5, and 1.0 as a function of temperature T at $H=800$ Oe. The solid line represents the calculated M from Eq. (1). (b) Schematic drawing of spin alignments in two neighboring LSMO and PSMO grains with the AFM type coupling.

The magnetization M of the $LSMO_{1-x}PSMO_x$ samples are evaluated and as an example, $M(T)$ under $H=0.8$ kOe at $x=0.1$, 0.5, and 1.0 is presented in Fig. 3(a). The measured M–H hysteresis indicated that the coercivity is just 70, 120, and 180 Oe, respectively, far lower than 0.8 kOe. Therefore, most spins in the sample should align in parallel to H at $H=0.8$ kOe. As reported, pure LSMO is in FM state overall T range, while pure PSMO starts the weak FM to AFM transition at 170 K and remains weak FM state over 170–280 K. The $LSMO_{1-x}PSMO_x$ as $x=0.5$ seems to be macroscopically ferromagnetic overall T range, leaving the superficial FM–AFM transition tail around 77 K. If no spin coupling and interfacial diffusion between neighboring LSMO and PSMO grains is assumed, one has magnetization M_{LP} for $LSMO_{1-x}PSMO_x$:

$$M_{LP}(T)=(1-x)M_L(T)+xM_P(T), \tag{1}$$

where M_L and M_P are the magnetization of LSMO and PSMO, respectively. The as-calculated $M_{LP}(T)$ is inserted in Fig. 3(a) for a comparison. The predicted M_{LP}–T and measured M_{LP}–T curves are very similar in shape but the former is ~1.5 times the latter below 210 K. The big difference at low T suggests strong spin coupling (AFM type) between the contacting LSMO and PSMO grains, by which the spins inside LSMO grains near the contacting boundaries prefer antiparallel alignment. As a simplified model, Fig. 3(b) gives a schematic of the intergrain spin coupling between LSMO and PSMO at low T. At zero field, the near-boundary layers in LSMO grains show antiparallel spin alignment due to the coupling. As H is not very high ($\sim 10^2$ Oe), some spins

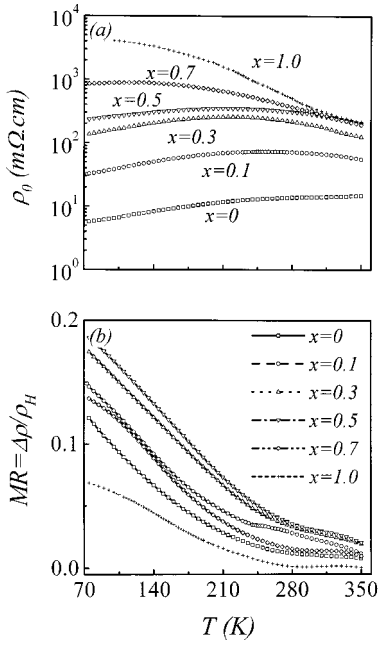

FIG. 4. Zero-field resistivity ρ_0 (a) and magnetoresistance $\mathrm{MR}=\Delta\rho/\rho_H$ (b) as a function of temperature T, respectively, for a series of $\mathrm{LSMO}_{1-x}\mathrm{PSMO}_x$ samples.

inside the layers remain antiparallel, so that the overall magnetization is smaller than the predicted by Eq. (1).

The VSM data also advise us that the interfacial diffusion between LSMO and PSMO grains in our samples is weak even if not excluded. The interfacial diffusion results in formation of $\mathrm{La}_{0.35}\mathrm{Pr}_{0.25}\mathrm{Sr}_{0.4}\mathrm{MnO}_3$ phase near the boundaries. This phase should be in paramagnetic insulating state at $T>\sim 200$ K and FMM state below ~ 200 K.[1] If the interfacial diffusion during the sample sintering dominants over the AFM coupling, the measured M_{LP} would be a little higher than that given by Eq. (1), which is not the case here.

Figures 4(a) and 4(b) present the measured zero-field resistivity ρ_0 and $\mathrm{MR}=\Delta\rho/\rho_H$ at $H=3.0$ kOe for a series of samples. The resistivity of $\mathrm{LSMO}_{1-x}\mathrm{PSMO}_x$ increases with increasing x. The position of T_m shifts leftward and reaches 250, 220, 210, 125, and <77 K as $x=0.1$, 0.3, 0.5, 0.7, and 1.0, respectively. Although ρ_0 as $x>0$ is higher than that as $x=0$, their difference is only one order of magnitude. The measured LFMR for $\mathrm{LSMO}_{1-x}\mathrm{PSMO}_x$ shows decaying with T. However, the decaying behavior over low T range up to 250 K is different from that of pure LSMO. The pure LSMO shows a rapid decaying LFMR with increasing T, with the decaying rate roughly proportional to T^2. The decaying is slowed down as $x=0.1-0.5$, and even slower for the PSMO-dominant samples ($x=0.7$) and pure PSMO. This effect is obviously attributed to the coupling between LSMO and PSMO and will be explained later. On the other hand, the enhanced LFMR for $\mathrm{LSMO}_{1-x}\mathrm{PSMO}_x$ as $x=0.1-0.7$, as compared to that of pure LSMO, is obtained. In order to understand the enhanced LFMR effect and its slow decaying with increasing T in $\mathrm{LSMO}_{1-x}\mathrm{PSMO}_x$ composites, one may consult Fig. 3(b). Because LSMO has better conductivity than PSMO, the current flows mainly through LSMO grains. The main part of LFMR is still attributed to the spin-polarized electron tunneling with grain boundaries as the barriers. Nevertheless, the induced coupling layers inside LSMO grains makes additional contribution to LFMR, which is responsible for the enhanced part of LFMR. At zero-field, the electron hopping across the coupling layers meets high resistance. The increased zero-field resistivity results from existence of PSMO and the antiparallel spin alignment inside the coupling layers. As a low field is applied, part of the spins inside the coupling layers realign along the field direction, resulting in enhanced electron hopping rate inside LSMO grains. This effect seems very significant in our system because of the very strong coupling. The temperature dependence LFMR for $\mathrm{LSMO}_{1-x}\mathrm{PSMO}_x$ composites can be qualitatively explained by the spin-polarized tunneling model $\Delta\rho/\rho_H=(1-\gamma)/(1+\gamma)P^2$, which takes into account of grain boundary tunneling,[11] where γ is the parameter to characterize the spin-flip scattering and local spin collective excitations from grain boundaries, P is the electron polarization. Since γ and P are the increasing the decaying function of T, respectively, the LFMR should decay with $.T$ at a rate of T^2. However, as revealed in Fig. 3, as H reaches up to 3.5 kOe, the AFM coupling between LSMO and PSMO grains collapses and the field-driven FM-like spin alignment is achieved, which benefits the local electron hopping and producing additional contribution to $\Delta\rho/\rho_H$. We denote by ΔM_{LP} the difference in magnetization for the coupling ranges at $H=0$ and 3.5 kOe. Referring to Fig. 3, ΔM_{LP} at $H=0.8$ kOe remains almost constant from 77 to 250 K. Therefore, decaying of $\Delta\rho/\rho_H$ with T thus is decelerated, in relative to term $(1-\gamma)P^2/(1+\gamma)$. As $T>250$ K, ΔM_{LP} decreases with increasing T and thus the decaying the LFMR becomes fast once more, as revealed in our experiment.

The authors acknowledge the financial support from NSF of China and the Key Projects for Basic Research of China as well as LSSMS of Nanjing University. J. M. L. is a Ke-Li fellow.

[1] *Colossal Magnetoresistance, Charge Ordering and Related Properties of Manganese Oxides*, edited by C. N. R. Rao and B. Baveau (World Scientific, Singapore, 1998).
[2] X. W. Li, A. Gupta, G. Xiao, and G. Q. Gong, Appl. Phys. Lett. **71**, 1124 (1997).
[3] S. Lee, H. Y. Hwang, B. I Shraiman, W. D. Ratcliff, and S. W. Cheong, Phys. Rev. Lett. **82**, 4508 (1999).
[4] C. Zener, Phys. Rev. **82**, 403 (1951).
[5] J.-M. Liu, J. Li, Q. Huang, L. P. You, S. J. Xu, C. K. Ong, Z. C. Wu, Z. G. Liu, and Y. W. Du, Appl. Phys. Lett. **76**, 2286 (2000).
[6] A. de Andres, M. Garcia-Hernandez, J. L. Martinez, and C. Prieto, Appl. Phys. Lett. **74**, 3884 (1999).
[7] L. Balcells, A. E. Carrillo, B. Martinez, and J. Fontcuberta, Appl. Phys. Lett. **74**, 4014 (1999).
[8] J.-M. Liu and C. K. Ong, Appl. Phys. Lett. **73**, 1047 (1998).
[9] M. Uehara, S. Mori, C. H. Chen, and S. W. Cheong, Nature (London) **399**, 560 (1999).
[10] B. Raveau, A. Maignan, C. Martin, and M. Hervieu, in *Colossal Magnetoresistance, Charge Ordering and Related Properties of Manganese Oxides*, edited by C. N. R. Rao and B. Baveau (World Scientific, Singapore, 1998), p. 43.
[11] P. Lyu, D. Y. Xing, and J. Dong, J. Magn. Magn. Mater. **202**, 405 (1999).